Acta Biomaterialia 14 (2015) 70–83

Contents lists available at ScienceDirect

Acta Biomaterialia

journal homepage: www.elsevier.com/locate/actabiomat

Revealing cytokine-induced changes in the extracellular matrix with secondary ion mass spectrometry

Adam J. Taylor [a,b,c], Buddy D. Ratner [c,d], Lee D.K. Buttery [a], Morgan R. Alexander [a,*]

[a] School of Pharmacy, University of Nottingham, Nottingham NG7 2RD, UK
[b] Department of Chemical Engineering, University of Washington, Seattle, WA 98195, USA
[c] National ESCA and Surface Analysis Center for Biomedical Problems, University of Washington, Seattle, WA 98195, USA
[d] Department of Bioengineering, University of Washington, Seattle, WA 98195, USA

ARTICLE INFO

Article history:
Received 22 August 2014
Received in revised form 22 November 2014
Accepted 8 December 2014
Available online 15 December 2014

Keywords:
ECM (extracellular matrix)
SIMS
Surface analysis
Osteoblast
Inflammation

ABSTRACT

Cell-secreted matrices (CSMs), where extracellular matrix (ECM) deposited by monolayer cell cultures is decellularized, have been increasingly used to produce surfaces that may be reseeded with cells. Such surfaces are useful to help us understand cell–ECM interactions in a microenvironment closer to the in vivo situation than synthetic substrates with adsorbed proteins. We describe the production of CSMs from mouse primary osteoblasts (mPObs) exposed to cytokine challenge during matrix secretion, mimicking in vivo inflammatory environments. Time-of-flight secondary ion mass spectrometry data revealed that CSMs with cytokine challenge at day 7 or 12 of culture can be chemically distinguished from one another and from untreated CSM using multivariate analysis. Comparison of the differences with reference spectra from adsorbed protein mixtures points towards cytokine challenge resulting in a decrease in collagen content. This is supported by immunocytochemical and histological staining, demonstrating a 44% loss of collagen mass and a 32% loss in collagen I coverage. CSM surfaces demonstrate greater cell adhesion than adsorbed ECM proteins. When mPObs were reseeded onto cytokine-challenged CSMs they exhibited reduced adhesion and elongated morphology compared to untreated CSMs. Such changes may direct subsequent cell fate and function, and provide insights into pathological responses at sites of inflammation.

1. Introduction

The extracellular matrix (ECM) is known to be a key director of the fate, behavior and function of cells and tissues. Cells may sense surface composition, topology and mechanical properties of the ECM. Through complex signaling pathways, these may influence cell activities as diverse as cell adhesion, contractility, morphology and gene expression. These, in turn, drive phenotypic characteristics and regulate the remodeling of the ECM itself. In many inflammatory disorders, changes to ECM composition and structure drive both disease progression and severity [1,2]. For example, in inflammatory environments the action of cytokines such as interleukin (IL)-1β, tumor necrosis factor (TNF)-α and interferon (IFN)-γ disrupt matrix homeostasis by reducing ECM deposition and enhancing ECM resorption. Simultaneously, altered ECM deposition in inflamed tissues can actively influence immune responses at such sites [3].

The influence of the ECM on cell behavior can be challenging to investigate experimentally in a biologically relevant manner. Adsorbed protein surfaces have been widely used, although they only provide a flat, adhesive surface that does not approach the complexity of native ECM. Many developments have been made in the production of decellularized tissues and organs [4–6], their characterization [5,7,8] and developing use in the clinic [9–11]. However, whilst matrices may be produced from different tissue sources, anatomical locations, disease models or species, given their in vivo source, little control over matrix composition and structure at the point of deposition is possible. Therefore, the production of in vitro cell-secreted matrices (CSMs), where cells of interest are stimulated to deposit an ECM in situ before decellularization, providing a surface that may mimic in vivo niche environments, have been increasingly reported, with the aim of more closely recapitulating the in vivo environment.

* Corresponding author. Tel.: +44 115 951 5115; fax: +44 115 951 5102.
E-mail address: morgan.alexander@nottingham.ac.uk (M.R. Alexander).

http://dx.doi.org/10.1016/j.actbio.2014.12.005
1742-7061/

CSMs, also referred to in the literature as cell-derived matrices, have been produced from a range of cell types, including mesenchymal stem cells [12–16], hematopoietic stem/progenitor cells [17], epithelial and endothelial cells [18], fibroblasts [19,20], hepatic cells [21] and osteoblasts, both primary [22,23] and from cell lines [24]. They have found a number of applications, from early studies to understand cell proliferation and migration [19,25], to later studies investigating how the ECM directs stem cell differentiation [14,16,26]. CSMs have also been used to understand a number of disease states, notably examining cancer cell migration and metastasis [23,27–30], and genetic bone diseases exhibiting abnormal matrix deposition [22]. Recent studies report the use of CSMs in a broad range of studies, including those of vascularization [31], mesenchymal stem cell (MSC) differentiation [32] and cell migration [33]. A key advantage of CSMs is that they may be manipulated or modified at multiple points during their deposition. This may be through selection of cell types [22,26], culture conditions [14], differentiation protocols or post-decellularization modification [22,26].

Most commonly, CSM surfaces have been studied in situ by immunocytochemical and histological techniques [15,22], or ex situ, solubilizing the ECM before analysis by immunolabeling techniques such as enzyme-linked immunosorbent assay (ELISA) or Western blotting. For example, Bhat et al. [22] used immunohistochemistry to reveal increased levels of ECM components in CSMs from osteoblasts from donors with the genetic bone disease craniosynostosis compared to healthy donors. Whilst these approaches may be used to identify specific components, prior knowledge is required to select and identify appropriate targets. Spectroscopic and spectrometric techniques are useful as they collect data representative of the sample as a whole, rather than targeting specific components. Recently, proteomic methods employing mass spectrometry have been used to study CSMs and decellularized tissues [34], including the identification of novel matrix components from CSM secreted by a fibrotic liver cell line [21]; a comparative analysis of CSMs that support or inhibit the maintenance of pluripotency in human embryonic stem cells [35]; and proteomic analysis of decellularized human vocal fold mucosa [36]. However, such approaches require solubilizing the sample, removing one of the advantages of CSM systems – that the ECM proteins are presented at the surface in their native "as-secreted" orientations and structures. Therefore in situ surface analytical methods are advantageous.

Time-of-flight secondary ion mass spectrometry (ToF-SIMS) is a surface analytical technique that has been widely used to study a range of biological samples, including proteins [37–40], lipids [41], DNA microarrays [42] and cultured cells [43,44], along with "soft" [45–47], "hard" [48] and decellularized tissues [7,8]. In ToF-SIMS a primary ion beam (in this study Bi_3^+) is used to impact the surface of interest, yielding characteristic fragments from the top few nanometers of the surface. A proportion of these fragments are charged ions and may be analyzed using a time-of-flight detector to yield mass/charge spectra characteristic of the surface. From these spectra information may be extracted about the chemistry [49], structure [50] and molecular orientation [51] of the surface. ToF-SIMS provides certain advantages in the analysis of biological materials over both other proteomic mass spectrometry based methods and traditional biochemical techniques. Notably, ToF-SIMS allows surfaces to be analyzed in situ without digestion or disruption of the surface; and does not require a priori selection of targets of interest. When proteins are analyzed by ToF-SIMS, the positive ion spectra are dominated by their amino acid building blocks and associate molecular fragments [37]. The study of amino acid homopolymers [52,53] has allowed characteristic peaks for each amino acid residue to be identified, and this information can be used to probe the nature and orientation of proteins at interfaces [37].

Multivariate analysis techniques are useful to aid the interpretation of data from complex, multicomponent surfaces [54]. These mathematical methods can be used to identify distinct groupings and subtle spectral differences in a large number of complex samples. Principal components analysis (PCA) is one multivariate technique that has been widely used to study protein-rich samples [7,37,55,56]. PCA has previously been used to distinguish spectra from adsorbed protein mixtures [37], decellularized tissues [7,8] or residual ECM proteins following cell lift-off [56,57].

With carefully decellularized surfaces and powerful analytical techniques available, this study sets out to: (i) use ToF-SIMS to identify differences in the composition of CSMs stimulated by exposure to the pro-inflammatory cytokines IL-1β and TNF-α and IFN-γ; (ii) compare findings from ToF-SIMS analysis with those from complementary biochemical techniques; and (iii) relate the structure of these CSMs to the behavior of cells reseeded on them.

2. Materials and methods

2.1. Cell culture

Mouse primary osteoblast cells (mPObs) were isolated from the calvariae of 1- to 3-day-old CD1 mice as described previously [58]. Briefly, calvariae were dissected and digested in a solution of 0.5 mg ml^{-1} trypsin II S (Sigma) and 1.4 mg ml^{-1} collagenase IA (Sigma). Cells released during the first two digestion periods (10 min each) were discarded. Cells collected from the subsequent three digestion periods (20 min each) were pooled and cultured at a density of 6.6×10^3 cells cm^{-2} in a basal medium consisting of minimum essential medium-α (Lonza) containing 10% fetal bovine serum (Sigma), 100 U ml^{-1} penicillin, 100 μg ml^{-1} streptomycin and 2 mM L-glutamine. Cells were passaged once before cryopreservation and used experimentally before passage 4.

2.2. CSM production

The mPOb cells were plated in basal medium on 12-well tissue culture treated polystyrene (TCP) multi-well plates or 13 mm diameter Thermanox coverslips (Thermo) at a density of 10,000 cells cm^{-2}. Cells were allowed to adhere overnight before culture in osteogenic medium consisting of basal medium supplemented with 50 mM beta-glycerophosphate, 50 μg ml^{-1} L-ascorbate-2-phosphate and, when cytokines were not present, 10 μM dexamethasone (all from Sigma, Inc.).

After 14 days, cultures were decellularized, but retained an intact ECM surface on the substrate. Cultures were washed gently with phosphate-buffered saline (PBS) before treatment with 20 mM ammonium hydroxide in water for 20 min at 37 °C with intermittent shaking, followed by a further gentle wash in PBS before treatment with 50 U ml^{-1} DNase I in PBS for 1 h at 37 °C. Subsequent to decellularization, CSMs were washed gently in PBS and allowed to soak overnight in PBS. CSMs were stored in PBS at 4 °C for no more than 2 weeks before use.

2.3. Cytokine challenge

Cytokine challenge medium was prepared by supplementation of osteogenic medium (without dexamethasone) with 1 ng ml^{-1} recombinant human IL-1β, 10 ng ml^{-1} human TNF-α and 100 ng ml^{-1} mouse IFN-γ (all R&D systems). Both IL-1β and TNF-α have cross-species reactivity between mouse and human, but IFN-γ does not. Control medium was not supplemented with

cytokines. After 7 or 12 days of mPOb culture for CSM production, cells were exposed to cytokine challenge medium or control medium for 48 h, before continuation of culture in osteogenic medium.

2.4. Protein coatings

As comparator surfaces, binary mixtures of collagen I and fibronectin were adsorbed onto TCP multi-well plates or Thermanox coverslips. For ToF-SIMS analysis, single protein solutions of rat tail collagen type I or bovine fibronectin (both Sigma) were prepared at 100 μg ml^{-1} in PBS. From these, 25:75, 50:40 and 75:25 volume:volume ratio mixtures were prepared. Thermanox coverslips (13 mm diameter) were covered with 500 μl of single protein solutions and mixtures before incubating for 1 h at 37 °C to allow for protein adsorption. The protein-coated coverslips were washed six times in ultrapure water and air dried before use. For cell culture experiments, single protein solutions of rat tail collagen type I or bovine fibronectin (both Sigma) were prepared at 10 μg ml^{-1} in PBS. From these, 50:50 volume:volume ratio mixtures was also prepared. All solutions were sterile filtered. Twelve-well TCP multi-well plates were covered with 500 μl of protein solution per well before incubating for 1 h at 37 °C to allow for protein adsorption. The protein-coated wells were washed twice in PBS before air drying and storage at 4 °C.

2.5. ToF-SIMS analysis

For ToF-SIMS analysis, CSMs were prepared as described previously on 13 mm diameter Thermanox coverslips, chosen for their stable support under decellularization. To remove residual salts and lipids, CSMs were immersed in 0.15 M ammonium acetate for 1 min with gentle agitation before dehydration through 20, 40, 60, 80 and 100% ethanol in water before air drying.

Samples were mounted on a flat stage with double-sided sticking tape, or in a back-mount stage and held in place by metal clips, before entry into the instrument. ToF-SIMS spectra were obtained for CSMs using an ION-ToF 5–100, and for adsorbed proteins using an ION-ToF 4–100. Both instruments were equipped with a Bi_3^+ liquid metal ion gun with an energy of 25 keV. The total ion dose was kept below 10^{12} ions cm^{-2} to ensure static SIMS conditions. The area of analysis was 500 × 500 μm, which was rastered in a random pattern across 256 × 256 pixels. Positive ion spectra were collected over the mass range of m/z 0–800. Spectra of negative ions were not collected as they yield less information from proteinaceous surfaces [4–6,14,37]. At least three replicates were prepared for each sample type, with at least three spectra obtained from separate sites on each replicate sample, yielding at least nine spectra per treatment condition. Positive ion spectra were calibrated against peaks for CH_2^+, CH_3^+, $C_3H_2^+$ and $C_4H_3^+$ before further analysis.

2.6. Principal components analysis

PCA performs an axis rotation to observe the variance in the data more clearly, set along new axes called principal components [54]. Two resulting plots are vital for interpretation: scores and loadings. The scores are a projection of the original data points onto the new axis (principal components) and reveal the relationship between samples in a given principal component. Loadings describe the rotation between the original axis and new principal components axis. They reveal the variables that are responsible for the separation seen in the scores plot. PCA was performed using the spectragui package of the NESAC/BIO MVA Toolbox running in MATLAB R2012a (The MathWorks, Inc.). Amino acid fragment peaks from the list previously used by Canavan et al. for analysis of ECM-surfaces [56] and adapted from work by Wagner and Castner [37] were manually identified using SurfaceLab 6 (ION-ToF) and selected in overlaid spectra from each sample set, before adding to a peak list. Using the statistics function, peak intensities were compiled into a single tab-separated text file. This was imported into spectragui. Sample names were created to group repeated samples together. Spectra were normalized against the total ion intensity of the peak set and scaled by square-root mean centering before principal components analysis was performed. The calculated scores and loadings were saved to the MATLAB workspace and plotted using Graphpad Prism 6.

2.7. F-Actin and DNA visualisation

To visualize the F-actin cytoskeleton, samples were fixed in a solution of 4% w/v paraformaldehyde (PFA) in PBS for 30 min, washed with several changes of PBS and permeabilized with 0.1% Triton X-100 in PBS for 30 min. The samples were then incubated with 66 nM AlexaFluor488 phalloidin (green) or AlexaFluor546 phalloidin (red, both Invitrogen) in a solution of 1% w/v bovine serum albumin (BSA) in PBS for 20 min at room temperature whilst protected for light. Where DNA staining was also desired, 1 μg ml^{-1} Hoechst 33258 (Invitrogen) was included with the phalloidin solution. Samples were then washed three times in PBS before imaging by fluorescence microscopy.

2.8. DNA quantification

Freshly prepared CSMs, or mPOb cultures prior to decellularization, were scraped into RIPA buffer (Sigma) on ice for 10 min. Standards of calf thymus DNA (Sigma) were made up in RIPA (radio-immunoprecipitation assay) buffer. Samples or standards were diluted as required in TE buffer (10 mM Tris–HCl, 1 mM EDTA, pH 7.5) and 100 μl was transferred to triplicate wells of black microplates. An equal volume of PicoGreen reagent (Sigma) diluted 1:200 in TE buffer was added. After incubation at room temperature for 5 min protected from light, the fluorescence intensity was measured at 480/520 nm (ex/em) with a microplate reader (Infinite 200 Pro, Tecan).

2.9. Immunocytochemistry

The ECM components collagen I and fibronectin were visualized by immunocytochemical staining. Samples were fixed in 4% (w/v) PFA for 20 min. After washing with PBS, samples were permeablized for 30 min with 0.1% Triton X-100 in PBS for 30 min and washed again in PBS, before blocking for 30 min with 1% (w/v) BSA in PBS supplemented with 3% (v/v) donkey serum. The blocking solution was removed and the primary antibody added without further washing. Primary antibodies used were rabbit anti-mouse collagen I polyclonal (Millipore, AB765P) and sheep anti-human fibronectin polyclonal (R&D Systems, AF1918). The primary antibody was allowed to incubate overnight at 4 °C. Subsequently, samples were washed with PBS (3 × 5 min) before incubation with the secondary antibody for 1 h at room temperature. Secondary antibodies used were donkey anti-rabbit IgG AlexaFluor488 conjugate or donkey anti-sheep IgG AlexaFluor546 conjugate (Both Invitrogen). Fluorescence microscope images were taken using a Leica DM-IRB inverted microscope and Volocity Imaging Software (Improvision).

Fibronectin content was quantified by ELISA. CSMs were scraped into RIPA buffer on ice for 10 min. The fibronectin concentration was determined using a fibronectin mouse ELISA kit (Abcam) according to the manufacturer's instructions and standardized against known concentrations of mouse fibronectin.

Percentage area coverage of collagen I was determined by image analysis of representative images of samples stained by

immunocytochemistry as described above. Representative images were thresholded manually in ImageJ to select positively stained areas only. Consistent thresholding parameters were used for all images. After conversion to a binary image, the percentage area was calculated using ImageJ's measure function, limiting the ROI to the threshold of the binary image.

2.10. Histology

Collagens and glycosaminoglycans were visualized by staining with Sirius Red and Alcian Blue. Samples were fixed in 10% (v/v) neutral buffered formalin in PBS for 20 min and rinsed three times with tap water before staining for proteoglycans with Alcian Blue solution (0.5% w/v Alcian Blue 8GX, 1% v/v acetic acid in distilled water) for 10 min. The samples were then rinsed in tap water for 1 min before staining in molybdophosphonic acid (1% w/v in distilled water) for 15 min. The samples were rinsed again in tap water before staining for collagens with Sirius Red solution (1% w/v Sirius Red 3B, 30% v/v saturated picric acid in distilled water) for 1 h. The samples were then rinsed once again and imaged immediately by bright-field microscopy.

Elution and absorbance measurement of dye from Sirius Red stained samples was used to quantify collagen content of CSMs. Formalin fixed samples were rinsed in tap water for 1 min before staining in Sirius Red solution (1% w/v Sirius Red 3B, 30% v/v saturated picric acid in distilled water) for 1 h. Samples were then rinsed in tap water and allowed to dry. The dye was eluted into a 50:50 v/v mixture of ethanol and 50 mM NaOH. Triplicate 100 µl samples were transferred to a 96-well multi-well plate and the absorbance at 540 nm was read using a microplate reader (Infinite 200 Pro, Tecan). The samples were calibrated against known concentrations of bovine collagen I dried onto multi-well plates before staining.

2.11. Total protein quantification

The total protein content of CSMs was determined using a micro-BCA protein assay kit (Thermo). Samples were collected with a cell scraper into RIPA buffer on ice and diluted as required in PBS. The micro-BCA assay was performed according to the manufacturer's instructions. Absorbance was measured at 526 nm using a microplate reader (Infinite 200 Pro, Tecan), and standardized against known concentrations of BSA in RIPA buffer.

2.12. Adhesion

mPOb cells were seeded at 10,000 cells cm^{-2} in serum-free basal medium onto cytokine-challenged CSMs, adsorbed proteins or untreated tissue culture polystyrene in 12-well plates. After 30 min or 2, 4 or 6 h, plates were washed three times with PBS to remove unadhered cells. The remaining live cells were stained with 4 µm calcein AM (Invitrogen) in basal medium for 30 min at 37 °C whilst protected for light. They were then washed in PBS before scraping into 200 µl of RIPA buffer on ice to lyse the cells and release fluorescent calcein. The fluorescence intensity of 100 µl lysate samples was measured at 494/517 nm (ex/em) using a microplate reader (Infinite 200 Pro, Tecan). The results were standardized against known cell numbers prepared by serial dilution.

2.13. Morphological assessment

The mPOb cells were seeded onto CSMs or adsorbed proteins at 5000 cells cm^{-2} in basal medium and incubated at 37 °C and 5% CO_2 for 24 h before PFA fixation and staining for the F-actin cytoskeleton as described previously. Representative fluorescence microscope images of F-actin stained samples were imported into ImageJ. Regions of interest (ROIs) following the perimeter of least 100 cells per sample image were manually selected using the wand (tracing) tool and measured using the Analyze Particles package. The cell spread area represents the area of each ROI. The aspect ratio is calculated as the ratio of the major axis length to the minor axis length for an ellipse fitted around the ROI. Scatter plots of cell area vs. cell aspect ratio were produced in R, displaying a density heat map to aid visualization of sub-populations.

2.14. Statistical analysis

All statistical analysis was performed in Prism 5 (Graphpad). Where only two groups were compared, an unpaired *t*-test was used. Where multiple comparisons were made, one- or two-way analysis of variance (ANOVA) was employed followed by Sidak's multiple comparisons test [59].

3. Results

3.1. Decellularization

The CSMs were produced by seeding mPObs on tissue culture plastic multi-well plates or Thermanox coverslips and culturing for 14 days in an osteogenic medium. Subsequently, monolayer cultures were decellularized in a two-step protocol using a low-concentration alkaline solution and a nuclease treatment. Staining of mPOb cultures prior to decellularization and CSM for both DNA and the F-actin cytoskeleton was performed, along with quantification of residual dsDNA and assessment of metabolic activity. Visible F-actin and DNA are eliminated by decellularization (Fig. 1A) and dsDNA levels are significantly (Fig. 1B, $p < 0.0001$, *t*-test) reduced, to 1.27 ± 0.154 µg cm^{-2} Calcein fluorescence seen on CSMs treated with calcein AM are significantly reduced compared to live, confluent mPObs prior to decellularization (Fig. 1C, $p < 0.0001$, *t*-test.). The fluorescence intensity of CSMs is less than 1% of that seen for mPObs, suggesting the almost total cessation of cellular metabolism by decellularization. As well as confirming the removal of cellular components, the retention of ECM components collagen I and fibronectin was assessed by immunocytochemical staining. In CSMs, both collagen I and fibronectin are seen as a dense fibrous matrix that appears little disrupted compared to mPOb cultures before decellularization, with little change in spatial distribution and level of staining (Fig. 1A). When observed by phase contrast microscopy, CSMs appear as a dense, intact network that adheres across the surface (Fig. 1A).

3.2. ToF-SIMS analysis

Representative positive ion ToF-SIMS spectra of CSM surfaces, model adsorbed protein films and the underlying Thermanox substrate, shown in Fig. 2, reveal a complex pattern of characteristic peaks. The spectra of the Thermanox substrate (Fig. 2C) can be easily visually distinguished from those from CSMs (Fig. 2D–F) and adsorbed proteins (Fig. 2A and B). Thermanox is understood to be a customized poly(ethylene terephthalate) (PET) resin subsequently functionalized to contain nitrogen-based groups to improve cell adhesion [60]. Many prominent peaks are known fragments of the PET backbone, including the PET repeat unit (*m*/*z* 193) and the benzoyl fragment $C_7H_5O^+$ (*m*/*z* 104), whilst others, not seen in the spectra of pure PET reported previously [61], can be identified as nitrogen-containing organic secondary ions, presumably resulting from proprietary modifications to PET, including negative ions *m*/*z* 26 and *m*/*z* 42.

The spectra of the proteinaceous surfaces analyzed are visibly distinct from that of the underlying Thermanox substrate. Positive

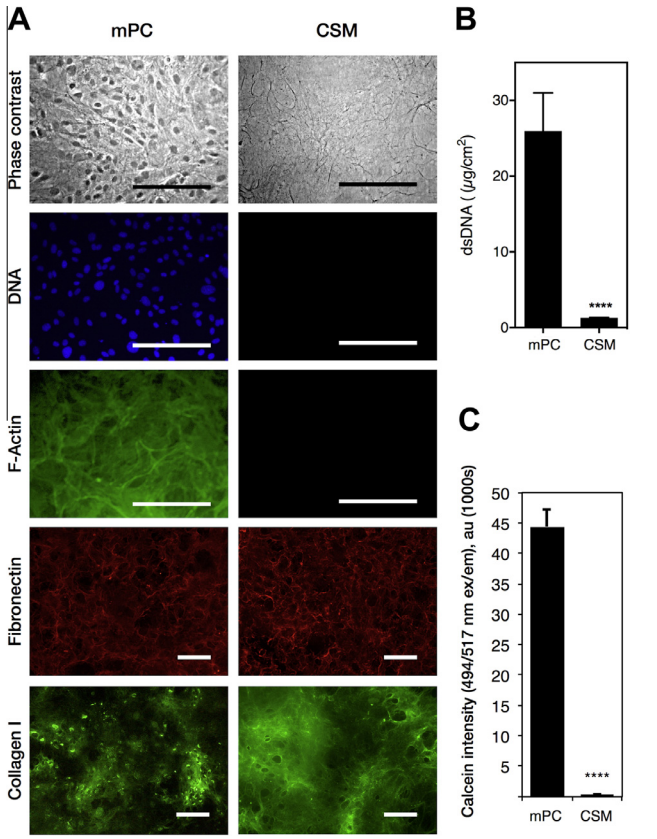

Fig. 1. (A) Representative phase contrast and fluorescence microscope images of CSMs before (left) and after (right) decellularization, stained for DNA (Hoechst) and F-actin (Alexa 488–phalloidin conjugate), along with immunocytochemical staining for fibronectin and collagen I. Scale bars represent 200 μm. (B) Quantification of dsDNA in CSMs before (left) and after (right) decellularization by PicoGreen assay. (C) Assessment of cell metabolic activity by calcein AM staining before (left) and after (right) decellularization. The bars in (B) and (C) represent mean ± 1 SD, $n = 3$. ****Significant difference, $p < 0.0001$, t-test.

ion spectra are dominated by peaks that have been identified as fragments associated with the amino acid building blocks of the proteins found at the surface, such as m/z 30 (common to all amino acids, although most characteristic of glycine) and m/z 43 and 59 (arginine). The prominent peak at m/z 70 found in all proteinaceous spectra is not unique to a single amino acid residue but may result from arginine, leucine or proline. Whilst it is possible to identify known fragments of individual amino acids in the spectra, the complexity of the ToF-SIMS spectra from proteinaceous surfaces makes it difficult to directly identify differences between samples of interest and associate differences with particular proteins. Therefore, PCA was used to identify differences in the intensities of known amino acid peaks in the positive ion spectra of the CSMs and adsorbed proteins. Fig. 3 presents scores and loadings plots for the first three principal components of all samples. The scores represent the relationship between samples, whilst the loadings reveal which peaks are responsible for the separation shown in the scores plot.

Principal component 1 (PC1) separates the as-received Thermanox substrate from all CSM surfaces and model protein coatings, and describes 90% of the variance in the data set. The associated scores plot (Fig. 3A) shows that PC1 gives high positive scores (0.39 ± 0.017, mean ± 1 SD) to sample points on the Thermanox substrate, whilst all other samples are scored negatively (min: −0.087; max: −0.023). The corresponding loadings plot (Fig. 3B) shows five peaks with positive loadings greater than 0.1 and 15 with negative loadings less than −0.1. Positively loaded peaks on PC1 include m/z 86 ($C_5H_{12}N^+$) and m/z 100 ($C_4H_{10}N_3^+$). Untreated Thermanox coverslips would not be expected to yield fragments of amino acid residues leucine/isoleucine (m/z 86) or arginine (m/z 100). Therefore, these peaks are likely products of nitrogen functionalization of the Thermanox detected at similar mass/charge values. Most of the remaining peaks from the peak list load negatively on PC1 towards the protein containing CSMs and adsorbed proteins.

Principal component 2 separates CSM surfaces significantly ($p < 0.0001$) from all model protein coatings and describes 6% of the variability within the data set. In the scores plot (Fig. 3C), CSM surfaces are scored positively (min: 0.030; max: 0.053) and are significantly different from all other groups ($p < 0.0001$). However, they are not significantly separated from one another ($p > 0.9$). The Thermanox substrate has a low positive PC2 score (0.0081 ± 0.0038). Adsorbed binary mixtures of collagen I and fibronectin are scored in decreasing order, moving from fibronectin, which is scored neutrally (−0.0024 ± 0.0045), to collagen I, with a high negative PC2 score. The corresponding loadings plot (Fig. 3D) shows that the majority of peaks have positive PC2 loadings greater than 0.1 (21 of 45). Only six peaks have negative PC2 loadings less than −0.1. These are peaks at m/z 68 ($C_4H_6N^+$ Pro), 70 ($C_4H_8N^+$ Arg/Leu/Pro), 73 ($C_3H_7N^+$ Arg), 115 ($C_4H_7N_2O_2^+$ Gly), 117 ($C_5H_9OS^+$ Met) and 127 ($C_5H_{11}N_4^+$ Arg).

Principal component 3 reveals significant differences between CSM surfaces with different cytokine challenge regimes. It describes 3% of the variability within the data set. In the scores plot for PC3 (Fig. 3E), all CSM surfaces are significantly separated from one another ($p < 0.05$). CSM surfaces produced with cytokine treatment on day 7 score neutrally (−0.0040 ± 0.0062), whereas those treated on day 12 have a more negative score (−0.019 ± 0.0077). CSM surfaces not treated with cytokines have the most negative scores of the three CSM surfaces (−0.026 ± 0.0035). The scores plot clearly and significantly separates the five collagen I/fibronectin model protein coatings in order, from pure fibronectin, with a high positive score (0.051 ± 0.0040), through mixtures moving from positive to neutral scores, to pure collagen I, with a high negative score (−0.038 ± 0.0068). The Thermanox substrate scores neutrally (−0.0031 ± 0.0070). The loadings plot for PC3 (Fig. 3F) highlights 10 peaks that exhibit positive loadings greater than 0.1. These include peaks that can be identified with the amino acids threonine (m/z 68, 74), valine (m/z 72), tryptophan (m/z 130, 159, 170) and tyrosine (m/z 136). Six peaks have negative loadings less than −0.1, five of which may be attributed to amino acid residues glycine (m/z 30), arginine (m/z 43, 100), proline (m/z 68) and leucine/isoleucine (m/z 86). The peak at m/z 44 may be associated with alanine or cysteine.

Plots for principal component 4 (PC4) and above are not shown. PC4 describes 0.954% of the variability in the data set. No significant separation between sample groups was observed in this or higher PCs, suggesting that this and further PCs describe variability within sample groups or noise within the data set.

3.3. Histological and immunocytochemical analysis

Whilst the composition of ECM secreted by cells cultured *in vitro* is too complex for all components to be identified using ToF-SIMS, ToF-SIMS has been demonstrated here to be a useful tool to identify the key compositional changes in CSMs. However, it is important to compare the conclusions drawn from ToF-SIMS spectra with those drawn from conventional biochemical techniques.

Quantification of the collagen mass in CSM surfaces through Sirius Red staining (Fig. 4B and A) reveals a significant decrease in collagens with cytokine treatment on day 7 of culture ($p < 0.0001$, two-way ANOVA with Sidak's multiple comparisons test) from 9.75 ± 1.05 μg in untreated CSMs to 5.45 ± 0.582 μg in treated CSMs (mean ± 1 SD) – a 44.1% reduction. No significant

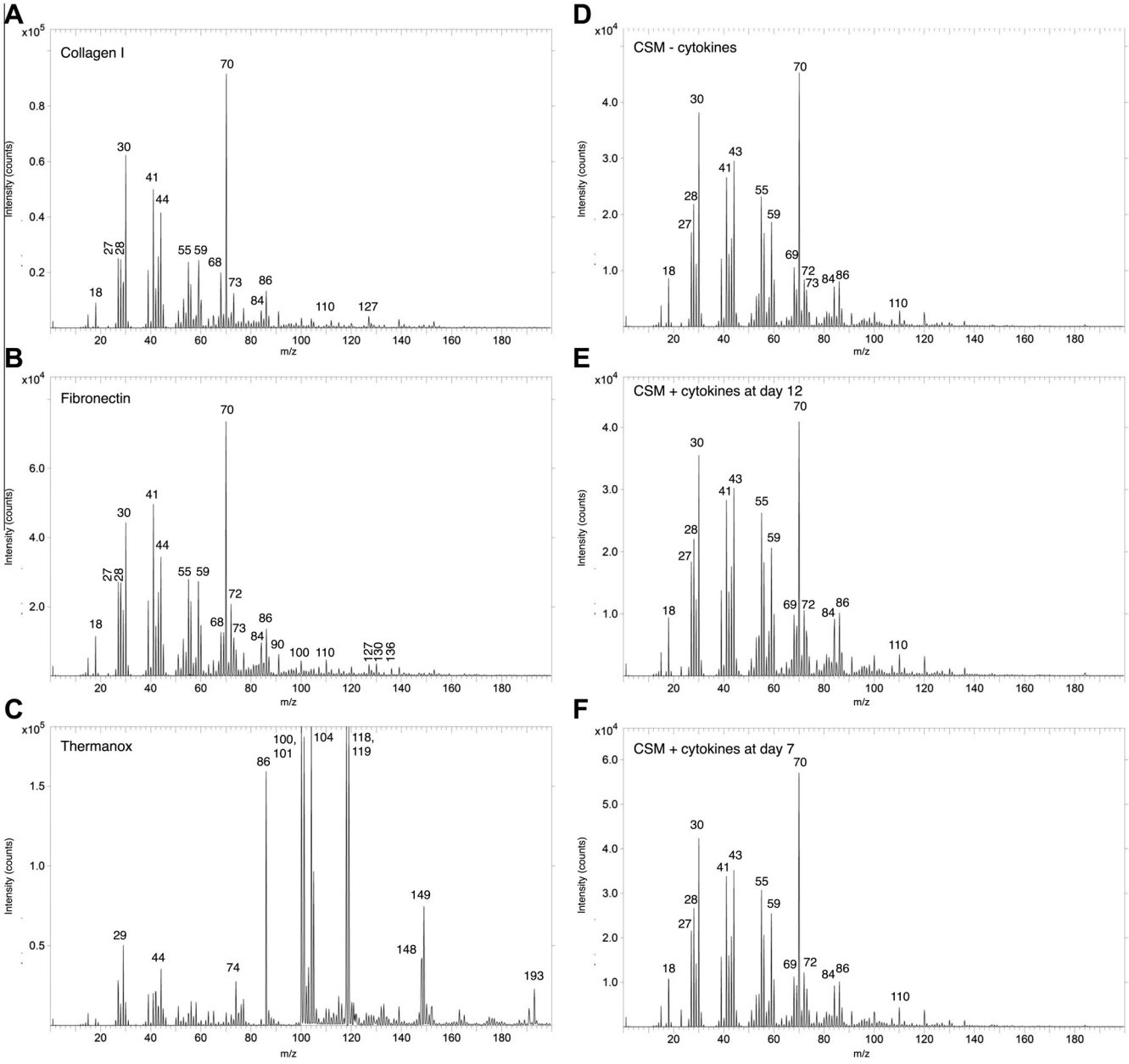

Fig. 2. Representative positive ion ToF-SIMS spectra obtained from CSMs with (D, E) or without (C) cytokine challenge, adsorbed collagen I (A) or fibronectin (B) coatings, or as-received Thermanox (C). Prominent peaks are labeled with their mass/charge.

difference in the collagen content of CSMs was observed with cytokine treatment on day 12 of culture ($p < 0.05$).

Representative bright-field microscopy images of CSM surfaces, stained with Sirius Red and Alcian Blue for collagens and glycosaminoglycans (GAGs) respectively, show a dense web-like network of collagens in untreated matrices (Fig. 4E). In matrices subjected to cytokine challenge at day 7, a notable disruption of the collagen matrix was observed, with areas of little or no staining. This does not appear to be seen with cytokine challenge at day 12. All CSM surfaces show positive staining for GAGs in a diffuse network of fibers. The GAG deposition or structure does not appear to be affected by treatment with cytokines at either time point.

Representative fluorescence microscope images of CSMs stained for collagen I (Fig. 4B) show that it is deposited in an interwoven, fibrous matrix, intact across the substrate. More staining is seen in CSMs not treated with cytokines, and it appears to be almost continuous across the surface. By comparison, there appears to be less staining in CSM surfaces treated with cytokines. This is particularly notable in CSM treated at day 7 of culture, where areas without collagen I staining can be seen. Additionally, the stained areas appear to be less organized than those seen in their untreated counterparts. Using image analysis to quantify the percentage area positively stained using consistent thresholding (Fig. 4A), a significant decrease in collagen I coverage is seen in CSM treated at day 7 compared to its untreated control ($p < 0.05$, two-way ANOVA with Sidak's multiple comparisons test), with coverage reduced from 76.9 ± 13.1 to 52.0 ± 10.70% (mean ± 1SD, $n = 3$) – a 32.4% reduction. No significant reduction in coverage is observed with cytokine treatment at day 12 ($p > 0.05$).

The total protein content of CSM lysates was determined by micro-BCA (Fig. 4C) and fibronectin was assayed by ELISA (Fig. 4F). No significant differences in total protein concentrations or fibronectin levels between CSM surfaces were found ($p > 0.05$, two-way ANOVA with Sidak's multiple comparisons test).

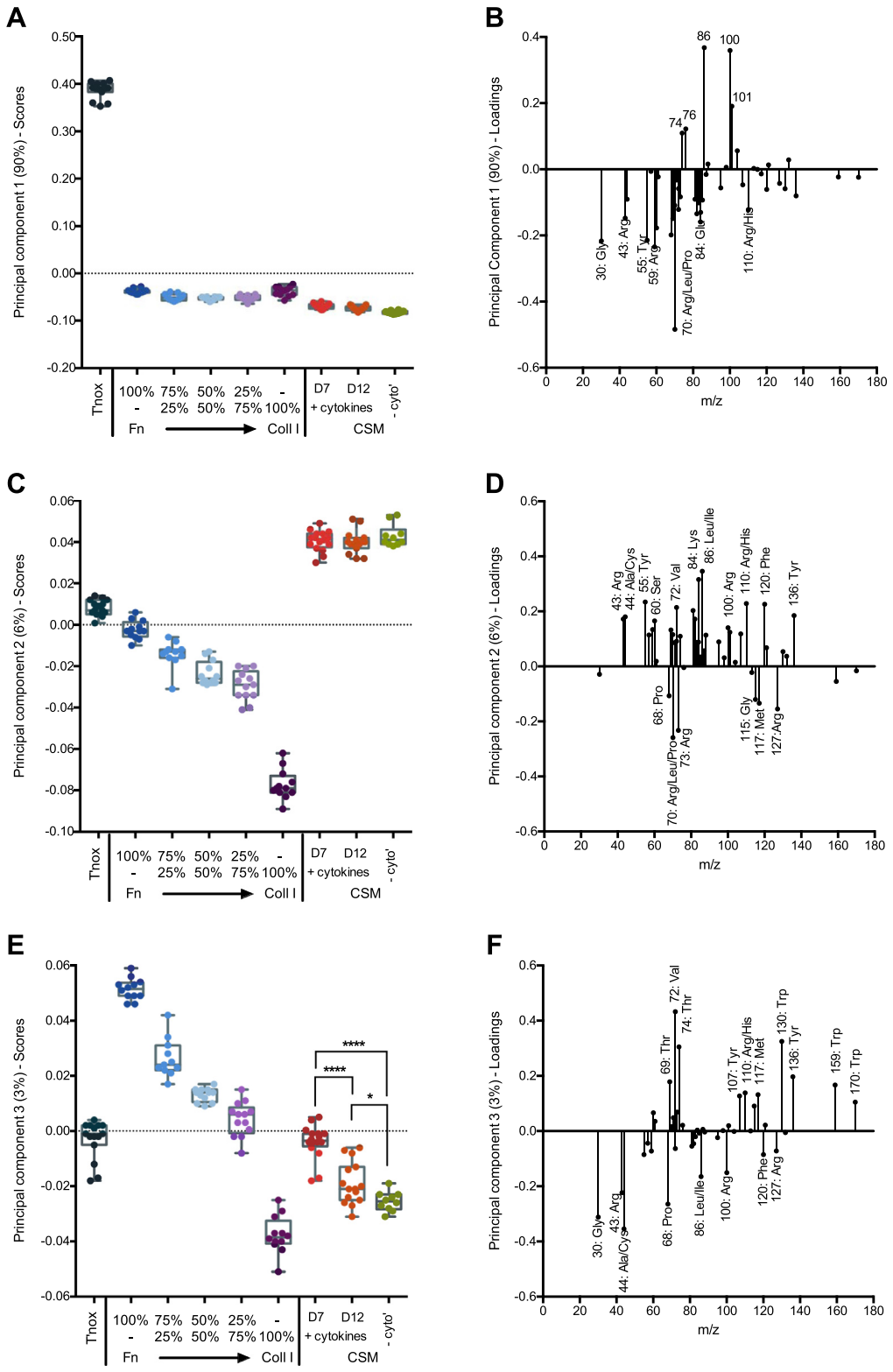

Fig. 3. Principal components analysis scores (left) and loadings (right) plots for principal components 1 (A, B), 2 (C, D) and 3 (E, F) from PCA of amino acid peaks selected from ToF-SIMS spectra obtained from as-received Thermanox coverslips (gray); adsorbed binary mixtures of fibronectin and collagen type I (blue through purple); and CSM surfaces with or without cytokine challenge (red = challenge at day 7, orange = challenge at day 12, green = no challenge). The scores plots (left) show individual sample scores, along with boxes marking median, 25th and 75th percentiles and whiskers marking minimum and maximum values. Notable significant differences are highlighted ($^{*}p < 0.05$, $^{****}p < 0.0001$, ANOVA with Sidak's multiple comparisons test). The scores represent the relationship between samples. In the loadings plots (right), highly loading peaks are labeled with their mass and assigned amino acid identity. The loadings show which peaks are responsible for the separation seen in the scores plots.

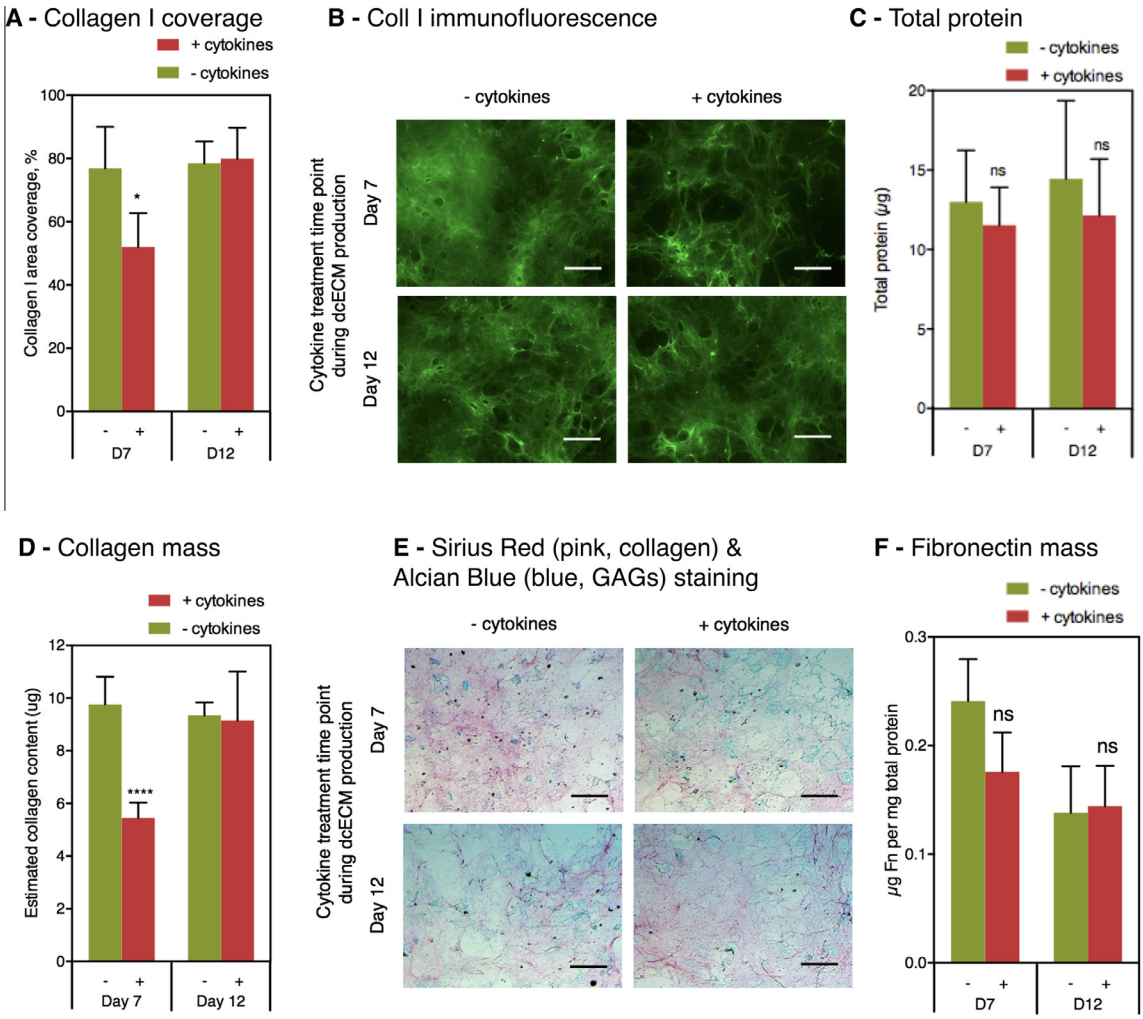

Fig. 4. (A) Quantification of collagen I surface coverage in cytokine-challenged CSMs assessed by image analysis of CSMs stained for collagen type I by immunofluorescence; representative images used are shown in (B). (C) Quantification of total protein in cytokine-challenged CSM surfaces by micro-BCA assay. (D) Quantification of collagen content in cytokine-challenged CSMs by elution of dye from Sirius Red stained samples. (E) Representative bright-field microscope images of CSMs stained with Alcian Blue (GAGs, blue) and Sirius Red (collagens, pink). (F) Quantification of the fibronectin content of cytokine-challenged CSMs by ELISA. In all plots bars represent mean ± 1 SD ($n = 6$). Significant differences between challenged and unchallenged CSMs are highlighted ($^{*}p < 0.05$, $^{****}p < 0.0001$, ns $p > 0.05$, two-way ANOVA with Sidak's multiple comparisons test). The scale bars represent 200 µm in all images.

3.4. Cell adhesion

The adhesion of mPOb cells to CSMs and adsorbed proteins was assessed under serum-free conditions (Fig. 5). At all time points studied, adhesion to pure collagen I was significantly lower than for either pure fibronectin or a 50:50 v:v mixture of collagen I and fibronectin ($p < 0.0001$, two-way ANOVA with Sidak's multiple comparisons tests). Cell adhesion was also significantly lower than on untreated tissue culture polystyrene at 30 min and 2 h. Adhesion to CSMs reached higher levels than for adsorbed proteins. The proportion of cells adhered to all CSM surfaces was significantly higher than all protein surfaces at the 2 and 6 h time points ($p < 0.001$). However, after 30 min, adhesion to all CSM surfaces was significantly lower than to pure fibronectin ($p < 0.001$), although the differences were not always significant for other CSM/protein comparisons at this time point.

Comparing the influence of cytokine challenge during CSM production on subsequent mPOb adhesion, significant decreases were observed at the 2 h ($p < 0.05$) and 6 h ($p < 0.0001$) time points between CSM surfaces exposed to cytokines at day 7 and their associated untreated comparator. Whilst significant, these differences remain small, with cytokine challenge at day 7 decreasing the percentage adhesion at 6 h from 73.48 ± 5.4 to 63.80 ± 4.9%. No significant differences in adhesion were noted when cytokine challenge occurs at day 12 of CSM production. Furthermore, no significant differences were observed between CSMs not treated with cytokines at day 7 or 12, indicating that these control groups are comparable ($p < 0.05$).

3.5. Cell morphology

Representative fluorescence microscope images of F-actin-stained mPOb cells seeded at sub-confluence onto CSMs or model proteins are shown as insets in Fig. 6. Clear morphological differences can be noted. Cells seeded onto CSMs appear more irregular in shape, more elongated and less spread than those seeded on proteins. The morphological characteristics of mPObs seeded at sub-confluence onto CSMs or model proteins were assessed by image analysis to quantify the cell spread area and aspect ratio. Fig. 6 shows these as scatter plots. Cells on CSMs (all groups) can be seen to have a significantly smaller cell spread area than those on collagen or a 50:50 v:v mix of collagen I and fibronectin ($p < 0.001$). Few cells on CSMs are seen with a spread area >4000 µm^2. Little difference in the distribution of cell spread area

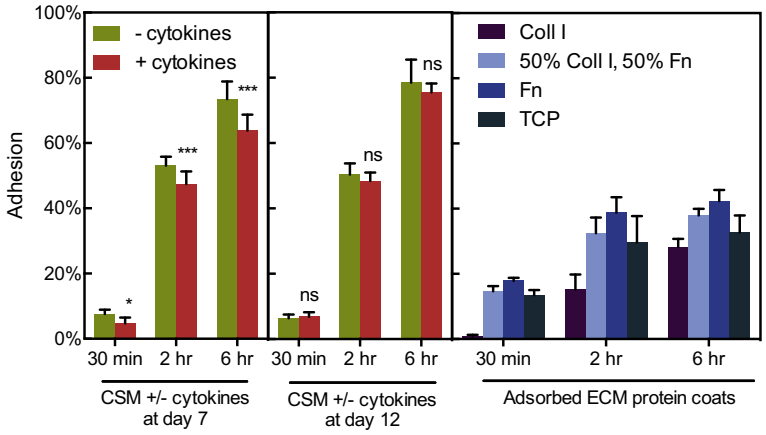

Fig. 5. Bar chart showing adhesion of mPOb cells to CSMs, with or without cytokine challenge (left), and adsorbed ECM proteins (right). mPOb cells were seeded in serum-free conditions at 10,000 cells cm^{-2}. After 30 min and 2 and 6 h, non-adhered cells were removed by washing in PBS and the remaining attached cells were quantified by staining with calcein AM. The fluorescence of calcein was normalized against known cell numbers. Bars represent mean ± 1 SD, $n = 6$. Significant differences in adhesion between treated and control matrices are highlighted ($^{*}p < 0.05$, $^{****}p < 0.0001$, ANOVA with Sidak's multiple comparisons tests).

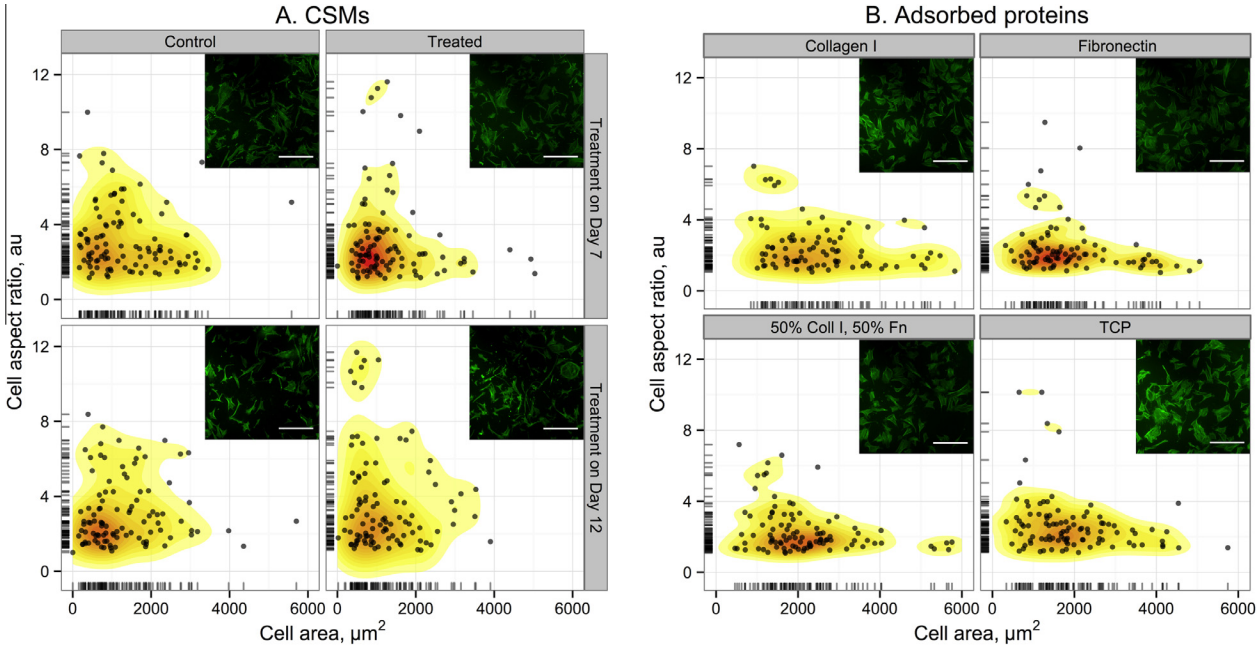

Fig. 6. Scatter plots showing cell area vs. cell aspect ratio (long axis/short axis) for mPOb cells seeded onto cytokine-challenged CSMs (A) or adsorbed proteins (B). Cells were seeded at 10,000 cells cm^{-2} for 24 h before fixing in PFA and staining the F-actin cytoskeleton with Alexa 488–phalloidin conjugate. Cells were imaged by fluorescence microscopy before manually bounding >100 cells per sample in ImageJ to calculate the cell area and aspect ratio. The heat map represents the probability density (low = white, high = red). Insets show representative images used for image analysis. Scale bars represent 200 μm.

is seen between CSMs exposed to different cytokine challenge regimes. However, some differences in the distribution of cell aspect ratios observed are noted. Whilst the majority of cells on all surfaces exhibit aspect ratios between 1 and 4, a notable number of cells on CSMs appear with elongated morphologies, with aspect ratios between 4 and 8. Few cells are seen with such elongated morphologies on adsorbed proteins or TCP. Scatter plots also reveal a number of very highly elongated cells with an aspect ratio of >9, observed only on CSMs exposed to cytokine challenge (either at day 7 or 12) during production. Cells with these morphologies are clearly separated from the bulk population, with very few cells observed with aspect ratios between 8 and 9. On CSMs not exposed to cytokines, few mPObs are seen with aspect ratios >8.

4. Discussion

4.1. Decellularization

First, we validated the effectiveness of the decellularization protocol. A key characteristic of decellularized matrices is that cellular components have been removed, while extracellular components and structure are retained [62]. For CSMs to be useful surfaces, they must also remain intact and adhere to the underlying substrate throughout decellularization, storage and subsequent use, as well as support the culture of relevant cell types [14,18].

In this study, a decellularization protocol of a low-concentration ammonium hydroxide treatment to lyse cells followed by a nucle-

ase treatment to remove residual nuclear material was used. Similar protocols have been reported previously, to produce CSMs from endothelial [63] and osteoblast cell types [23,24]. One of the most widely used decellularization protocols for the production of CSMs also utilizes ammonium hydroxide treatment, together with Triton X-100 detergent treatment [13,14,18,22]. Detergent treatment was not used in this study as decellularization appeared effective without its use. It has been suggested that detergent use may disrupt some ECM structures and components such as GAGs [62], whereas decellularization with ammonium hydroxide alone has been demonstrated to retain these components [24].

Staining for, and quantification of, DNA has been the most widely used and recommended assessment of decellularization effectiveness [62]. The CSMs produced in this study showed no visible DNA with Hoechst staining (Fig. 1A), and dsDNA levels were quantified to be under 1.5 μg dsDNA cm^{-2} (Fig. 1B). The removal of other cellular architecture, such as the F-actin cytoskeleton [18,64], and cessation of metabolic activity [14] have also been considered by earlier studies, and provide further validation of decellularization. The protocol used in this study was shown to effectively obliterate cytoskeleton, as assessed by F-actin staining (Fig. 1A). Additionally, elimination of intracellular esterase activity demonstrated the effective cessation of cellular metabolism (Fig. 1A).

Successful decellularization should not only remove cellular products, but also retain ECM components in a structural and conformational presentation close to that found prior to decellularization. Collagen I and fibronectin are key components of the ECM produced by osteoblasts, both in vivo, in the osteoid matrix that precedes mineralization, and in in vitro cultures. Immunofluorescence imaging shows that both are retained in CSMs in similar levels and structures to those seen prior to decellularization (Fig. 1A).

The matrix surface appears intact and continuous. Where damage or loss of matrix surfaces was observed, this tended to be seen at the lower edge of the matrix, where contact during the aspiration of medium or decellularization solutions was possible. As such, care was taken when preparing CSMs to avoid contacting the ECM surface. Others have reported similar challenges with matrix fragility [65]. Prewitz and co-workers [18] recently showed that covalent binding of fibronectin to a glass substrate significantly increased matrix robustness.

To assess the effects of pro-inflammatory cytokines on mPOb cultures being prepared for CSM surfaces, two cytokine challenge regimens were used. The combination of 1 ng ml^{-1} IL-1β, 10 ng ml^{-1} TNF-α and 100 ng ml^{-1} IFN-γ was selected on the basis of their reported synergistic effect and prior studies demonstrating their effectiveness in promoting an inflammatory response in mPObs [58]. This is the first study of CSMs produced following cytokine exposure, although Mountziaris et al. [66] had previously described the behavior of MSCs exposed to TNF-α and cultured on cell-derived matrices grown on acellular PCL/ECM scaffolds.

4.2. ToF-SIMS analysis

Having prepared and validated mPOb deposited CSMs from cytokine-challenged environments, ToF-SIMS analysis of both cytokine-challenged CSMs was performed. To test the hypothesis that collagen content is reduced by cytokine challenge, particularly at day 7, when there is time for matrix remodeling, CSM surfaces were compared to model proteins: specifically, mixtures of collagen I and fibronectin adsorbed onto Thermanox coverslips. Fibronectin was selected as a non-collagenous protein secreted by osteoblasts, critical for their differentiation [67] and survival [68], and demonstrated above to be present in the CSM surfaces. Fibronectin is readily identifiable by ToF-SIMS analysis due to its distinctive content of the cyclic amino acids tyrosine and tryptophan [39].

From examination of the raw ToF-SIMS spectra, it is difficult to distinguish between CSM groups and adsorbed proteins, both being formed predominantly of the same 21 amino acids, whilst the as-received Thermanox substrate is easily distinguishable (Fig. 2).

As with previous surface analytical studies of ECM samples [7,8,56,57], multivariate analysis is required to aid the identification of spectral differences between sample groups. To further simplify the number of variables (mass peaks) used for multivariate analysis and eliminate peaks from other components, such as the substrate or residual cellular material, these studies examined the intensities of specific peaks known to be characteristic of amino acid fragments.

Using an amino acid fragment peak list previously used to study ECM surfaces [57], PCA of cytokine-treated CSMs revealed spectral differences between surfaces from different treatment regimes, with CSMs treated at day 12 being more similar to untreated CSMs than those treated at day 7 (Fig. 3). Identification of highly loading peaks in PCA comparing both CSMs to each other and to model protein coatings, using a subset of known amino acid related peaks, suggests that these differences are due to the reduction in relative collagen content with cytokine treatment.

The first principal component separates the as-received Thermanox substrate from the other samples (Fig. 3A and B). As its spectral differences from the other samples are easily identifiable in the raw spectra, it is not surprising that the first principal component dominates the variance in the data set. With the peak list restricted to those thought to be characteristic of amino acids (i.e. supervised PCA), it is somewhat surprising that Thermanox yields secondary ions at these mass/charge ratios. However, proprietary nitrogen functionalization of the PET backbone, e.g. by gas plasma modification, could result in nitrogen-containing positive ion fragments with masses, structures and charges similar to several amino acid fragments.

Further discussing PC1, consideration of the substrate is important for ToF-SIMS analysis of thin samples or those of incomplete coverage. Here these are considered by including the bare substrate in the PCA. Some previous studies of ECM components on a poly(N-isopropyl acrylamide) (pNIPAM) substrate have included known substrate peaks [57,69], whilst in later studies from the same group these were not considered [56].

In principal component 2, which separates CSMs from adsorbed proteins (Fig. 3C), the large number of peaks loading positively, contributing to the high score of CSM surfaces compared to the few peaks loading negatively (Fig. 3D), illustrates the complexity of CSM surfaces compared to single proteins or binary protein mixtures. CSM surfaces contain many components that have been secreted and remodeled by a population of cells in response to their environment. These may include structural ECM proteins such as elastin, or ECM proteins, such as osteopontin or osteocalcin, that are involved in osteogenesis and maturation from a collagen-rich osteoid matrix to mineralized bone-like nodules. In comparison, the defined components and controlled adsorption conditions of the model protein coatings make them simpler surfaces than CSM, with known composition and homogeneous spatial distribution and orientation – all surface characteristics that may influence the resulting spectra. Whilst binary mixtures of collagen I and fibronectin can be separated from one another, PC2 does not allow CSM surfaces to be distinguished according to cytokine exposure.

Comparing the scores in PC3 with those for model protein mixtures, it can be seen that CSM surfaces are collagen rich, displaying scores between those for 100% collagen I and a 75:25 collagen I:fibronectin ratio (Fig. 3E). Untreated CSM surfaces score more

towards the pure collagen sample than those treated with cytokines, which score towards fibronectin-containing protein mixtures. This suggests that untreated CSM shares more spectral similarities with pure collagen than those exposed to cytokine challenge. The neutral scoring of the Thermanox substrate indicates that it does not contribute to the peaks seen in the loadings plot for PC3 (Fig. 3F).

In summary, principal components analysis of cytokine treated CSMs allows for the identification of distinct spectral differences between surfaces from different treatment regimes, with CSMs treated at day 12 being more similar to untreated CSMs than those treated at day 7. Identification of highly loading peaks in PCA comparing both CSMs to each other and to model protein coatings using a list of known amino acid-related peaks suggests that these differences are due to the reduction in relative collagen content with cytokine treatment.

Assessment of the composition of complex protein-rich surfaces is challenging. Whilst proteomics-based techniques allow detailed and accurate compositional analysis, and have been employed to study a range of decellularized systems, including CSMs [21,34–36], they typically require sample digestion. ToF-SIMS, on the other hand, allows for samples to be examined as deposited – retaining their natural structure and conformations. Although ToF-SIMS can be used to readily identify components in single [37] and binary [39] adsorbed protein systems, it is difficult to quantitatively assess the composition of multicomponent protein surfaces. However, it is possible to describe qualitative trends through comparison with reference protein spectra [38]. This approach has been taken by the few studies that have reported ToF-SIMS analysis of ECM-based systems. Two sequential studies performed ToF-SIMS analysis of decellularized tissues, including oesophagus, bladder, small intestine and liver. PCA using an amino acid peak list was able to distinguish samples by both anatomical location and method of preparation [8]. Separate PCAs of decellularized tissues and model proteins were qualitatively compared and associated with tissue origin, although no conclusions on the identification of ECM components were drawn [7].

In another series of studies, multivariate analysis of ToF-SIMS data allowed for pNIPAM-coated tissue culture polystyrene after thermal cell-sheet lift-off to be distinguished from both the underlying substrate and surface modification [57]. By deriving principal components from model proteins alone to form a model into which data from surfaces of interest were projected, the residual ECM could be associated with laminin, as opposed to fibronectin or collagen [56]. Whilst such surfaces may not be considered as true decellularized matrices, as their purpose is to release intact and viable cell sheets from the surface, leaving some residual extracellular components, rather than to retain ECM structures for subsequent experiments, they nevertheless provide a useful comparator to the CSMs presented here.

Whilst the compositions of ECMs naturally produced in vitro are too complex for all of their components to be identified using ToF-SIMS, it has been demonstrated to be a useful tool to identify key compositional changes. In order to confirm these conclusions, it is necessary to compare them with standard biochemical techniques.

4.3. Validation of ToF-SIMS conclusions with biochemical techniques

Inspection of CSMs treated with pro-inflammatory cytokines at day 7 of culture when stained with Sirius Red and Alcian Blue (Fig. 4E) or by immunofluorescence for collagen I (Fig. 4B) showed that cytokine treatment disrupts the level and distribution of collagen content. However, no significant difference is seen with cytokine challenge at day 12. These results validate the conclusions reached from ToF-SIMS data that cytokine challenge at day 7 of matrix production leads to a reduction in collagen content compared to untreated matrices, whilst when cytokine challenge takes place at day 12 there is less change in collagen content. After 12 days of osteogenic culture, mPObs are expected to exhibit a more mature osteoblastic phenotype than after only 7 days of culture. This more mature phenotype may be more resistant to cytokine challenge. Additionally, CSMs exposed to cytokine challenge at day 12 had little time for altered ECM deposition to occur prior to decellularization on day 14.

No significant change in total protein content of CSM surfaces is seen with cytokine challenge at either time point (Fig. 4C). A reduction in the collagen content but maintenance of the overall protein content would suggest that levels of another non-collagenous ECM protein may be elevated. However, no significant increase in fibronectin content is observed by ELISA (Fig. 4F).

Previous studies in primary calvarial cells [70] and MC3T3-E1 cells [71] showed that exposure to TNF-α alone could reduce collagen production by 30–35%. Stimulation with IL-1β alone decreases collagen deposition in both MC3T3-E1 cells [72] and the osteosarcoma cell line MG-63 [71]. These studies support the drop in collagen identified from ToF-SIMS analysis and the subsequent quantification of a 44.1% reduction in collagen content in CSM after exposure to a cocktail of pro-inflammatory cytokines at day 7 in our model.

Whilst several studies have suggested that IL-1β [72] and IFN-γ [73] induce a slight decrease in non-collagenous protein expression by bone cells, no significant decrease in fibronectin or total protein content was seen in CSMs produced after exposure to a combined cocktail of cytokines at early or late time points.

The mechanisms of action of IL-1β, TNF-α and IFN-γ have been well described. These pro-inflammatory cytokines are understood to influence the ECM through multiple pathways, including the down-regulation of collagen I gene expression [74,75]. TNF-α in particular has also been shown to disrupt collagen fibril assembly [76]. Additionally, cytokines, including IL-1β and TNF-α, are known to promote expression of a range of matrix metalloproteases (MMPs), many of which exhibit collagenolytic activity [3,77]. Whilst IFN-γ has been shown to down-regulate several MMPs, the synergistic effect these cytokines in bone cells has been demonstrated to result in a loss of collagen [78]. Reduced percentage area and increased heterogeneity of collagen I coverage may potentially be explained by the action of MMPs to actively degrade previously deposited ECM, although their presence or activity was not investigated here. Not all ECM components are down-regulated by inflammatory cytokines. The deposition of proteoglycans, including decorin, biglycan and versican, which both act to structurally organize the ECM and are part of complex transduction networks for inflammatory signals, are increased in fibroblasts treated with IL-1β and TNF-α [79]. Decorin expression is increased in smooth muscle cells treated with IL-1β. Whilst not explored in this study, it may be hypothesized that cytokine-induced proteoglycan synthesis is a factor in the maintenance of total protein levels observed in cytokine-challenged CSMs.

4.4. Adhesion of reseeded mPOb cells

As the initial interaction between seeded cells and a surface, adhesion plays an important role in subsequent cell behavior. On proteinaceous surfaces, this is mediated by the interactions of cell binding ligands with specific amino acid binding motifs found in the surface's constituent proteins. The serum-free adhesion of mPOb cells was higher on CSM surfaces than on any single ECM protein or binary mixture. Whilst the adsorbed protein coats will present appropriate binding motifs, their homogeneous nature may mean that these sites are sub-optimally oriented or available for integrin interactions. CSMs, however, are deposited in situ in a

complex structure of fibers and bundles determined by the secreting cell population, and therefore may present binding sites with better accessibility and availability. Additionally, CSMs contain a wide mixture of components, some of which may complement and assist in cell binding. Differences in the adhesion of mPOb cells to different adsorbed protein mixtures were observed (Fig. 5). Adhesion was consistently lowest on pure collagen I and highest on pure fibronectin, with the 50:50 v:v binary mixture showing intermediate adhesion, corresponding to previously reported results [80]. This is likely due to differences in the rate of integrin binding. Binding to collagen I is predominantly through the $\alpha1\beta1$ and $\alpha2\beta1$ integrins, whilst fibronectin binding is mediated through the interaction of a range of integrins with the Ar–Gly–Asp (RGD) motif [81]. Mixed formulations may not perform as expected for simple binary mixtures as collagen I contains a specific fibronectin binding site that regulates fibronectin fibril formulation, possibly leading to more complex interactions between the two components [82].

A small but significant decrease in cell adhesion is seen between CSMs exposed to cytokine challenge at day 7 and their control. A similar difference is not observed with cytokine challenge at day 12. This difference in adhesion may be due to several changes in the CSM induced by exposure to cytokines during deposition. The drop in collagen content and increase in the heterogeneity of distribution caused by cytokine challenge, demonstrated earlier, may result in decreased density of binding motifs in collagen I available for integrin binding or the distortion of ECM structure and potentially other related parameters, including mechanical and topological properties, leading to concealed or obscured binding sites. It has recently been shown that cell adhesion is dependent on the matrix fiber stiffness, orientation and available adhesive area [83]. Alternatively, cytokine treatment may have damaged other ECM components that support cell binding, such as fibronectin, with its extensive RGD motifs. Although beyond the scope of the present investigation, these hypotheses may be tested in future studies through the use of integrin blocking or knockdown experiments.

4.5. Morphology of reseeded mPOb cells

When seeded at sub-confluence to minimize cell–cell interactions, mPOb cells were shown to present a smaller spread area and higher aspect ratio on CSM surfaces (Fig. 6A) than on adsorbed proteins (Fig. 6B), although many cells remained rounded (aspect ratio <3). A large number of cells were seen with more elongated aspect ratios. This corresponds with previously reported studies of cell morphology on CSMs [84].

Cell spreading and aspect ratio may be controlled by a range of surface parameters, including, but not limited to, ECM composition, stiffness and ligand dentistry, topographic roughness and alignment, ECM restriction, porosity, elastic behavior and crosslinking, and may influence cell–cell signaling, cell contractility, cell adhesions and cell motility [85]. CSMs present a fibrous surface rather than the homogeneous relatively flat surface of adsorbed proteins. Alignment of cells along these structures, through both preferential movement and spatial restriction, can be seen to result in elongation of cell shape. Additionally, the presumably more heterogeneous distribution of binding ligands in CSMs may lead to contortion of cell shape as focal adhesions are formed.

On CSMs not exposed to cytokines, mPObs reach a maximum aspect ratio of ~8. However, on CMSs that did see cytokine challenge, both at day 7 and at day 12, a notable cluster of small, highly elongated cells is noted. This cluster, representing <7% of cells, is clearly separated from the bulk population. Importantly, biochemical analysis could not identify a significant difference between CSMs with or without cytokine treatment at day 12. However, ToF-SIMS analysis was able to separate these matrices, indicating both the advantages of sensitive surface analysis techniques and that the mechanisms causing this difference in cell behavior may be more complex than a simple alteration of ECM composition and collagen distribution.

Considering the effects of cytokine treatment on osteoblast CSM as previously discussed, it is possible to hypothesize as to the cause of this morphological cluster. First, it may be due to areas of decreased availability of specific binding ligands, either through decreased density or by deactivation through cryptic or unfolding mechanisms [86]. Equally, cytokine challenge may alter levels of ECM crosslinking, which may control folding and stretching in new ECM deposited by reseeded cells as they interact with the matrix [87]. Previous studies have demonstrated that decreased collagen density may yield an increased cell aspect ratio and a decreased surface area, increasing the number of projections of fibroblasts [88]. Decreased collagen coverage prompted by cytokine challenge may increase the size of lacunar area (areas without matrix), and hence between available collagen I binding sites. Supporting this hypothesis, Dumas et al. [89] showed that mechanical stimulation during CSM production increased matrix lacunar areas, leading to a subsequent decrease in cell circularity. In synthetic studies, altering the spacing and size of protein islands may manipulate the cell morphology by controlling integrin clustering and focal adhesion maturation [90,91]. Secondly, possible changes to ECM topology may lead to localized spatial restriction of cells as they align to features of the matrix. A variety of synthetic systems have shown how topography, both random and aligned, can direct cell morphology [92]. In a CSM system, Cukierman et al. [93] showed that flattening matrices with a weight increased the cell spread area and reduced the aspect ratio of reseeded fibroblasts. Thirdly, changes to ECM stiffness or elasticity may also come into play. The fibrous nature of ECM can result in complex non-elastic, viscous behavior [94]. Prewitz and co-workers [18] showed that CSMs from different culture environments exhibit significantly different Young's moduli. It is likely that all of these mechanisms, and more, contribute to the effects observed. Although not investigated in this study, these factors could be considered through the comparison of cell behavior on CSMS to that on other quasi-vivo substrates such as Matrigel, or synthetic substrates with controlled stiffness and topography. The possibility that the observed changes in both morphology and adhesion are the effects of an inflammatory response to residual cytokines, entrapped within the matrix from prior cytokine challenge and retained post-decellularization, must be considered as a potential confounding factor. Previous studies have shown that growth factors, including bone morphogenetic proteins and vascular endothelial growth factor, may be retained in CSMs [23,24]. However, preliminary studies to measure the inflammatory marker nitric oxide on mPOb cells reseeded on cytokine challenged showed this to be not significantly different from baseline (data not shown), suggesting that this is not a confounding effect on the conclusions drawn here.

5. Conclusions

This study has demonstrated the production of CSMs from mouse primary osteoblasts exposed to cytokine challenge during matrix deposition. CSMs were found to be cell free, and to retain relevant ECM components and structure. Analysis of ToF-SIMS spectra obtained from CSMs allows the different cytokine challenge regimes to be differentiated. Comparison with adsorbed protein mixtures of collagen I and fibronectin suggest that the spectral differences between matrices produced with and without cytokines are associated with a loss of collagenous proteins. This is confirmed by histology and immunocytochemistry, demonstrating a drop in collagen coverage and mass in CSMs exposed to cytokine

challenge midway through matrix deposition. These differences in ECM composition and structure were demonstrated to influence the adhesion and morphology of cells reseeded on cytokine-challenged matrices, which may direct subsequent cell fate and function.

The production and analysis of novel CSMs from simulated inflammatory environments demonstrated in this study further highlights the utility of CSM systems to investigate ECM-based disease states. This work provides insights into the effect of cytokines involved in inflammation on ECM composition and structure, as well as subsequent cellular behavior. It builds on previous surface analytical studies of ECM materials and represents the first investigation of CSMs by ToF-SIMS. It also provides a basis for further application of surface analytical techniques to examine a range of decellularized systems.

6. Disclosures

The authors declare no potential conflicts of interest.

Acknowledgements

The authors would like to acknowledge the funding of the EPSRC Doctoral Training Centre in Regenerative Medicine (EP/F500491/1), the UWEB21 program, and the facilities provided by the National ESCA and Surface Analysis Centre for Biomedical Problems (NESAC/BIO, NIH grant EB-002027) at the University of Washington. M.A. gratefully acknowledges The Royal Society for the provision of his Wolfson Research Merit Award. The authors thank Dan Graham (University of Washington) for developing the NESAC/BIO Toolbox used in this study, and are grateful for the advice and assistance provided by David Castner and Lara Gamble (University of Washington), David Scurr, Glen Kirkham and Laura Sidney (University of Nottingham), and Julia Kokesch-Himmelreich (Justus Liebig University Giessen).

Appendix A. Figures with essential color discrimination

Certain figures in this article, particularly Figs. 1, 3–6 are difficult to interpret in black and white. The full color images can be found in the on-line version, at http://dx.doi.org/10.1016/j.actbio.2014.12.005.

References

[1] Hardy R, Cooper MS. Bone loss in inflammatory disorders. J Endocrinol 2009;201:309–20.
[2] Walsh NC, Crotti TN, Goldring SR, Gravallese EM. Rheumatic diseases: the effects of inflammation on bone. Immunol Rev 2005;208:228–51.
[3] Sorokin L. The impact of the extracellular matrix on inflammation. Nat Rev Immunol 2010;10:712–23.
[4] Brown BN, Freund JM, Han L, Rubin JP, Reing JE, Jeffries EM, et al. Comparison of three methods for the derivation of a biologic scaffold composed of adipose tissue extracellular matrix. Tissue Eng Part C 2011;17:411–21.
[5] Badylak SF, Weiss DJ, Caplan A, Macchiarini P. Engineered whole organs and complex tissues. Lancet 2012;379:943–52.
[6] Gilbert TW, Sellaro TL, Badylak SF. Decellularization of tissues and organs. Biomaterials 2006;27:3675–83.
[7] Barnes CA, Brison J, Michel R, Brown BN, Castner DG, Badylak SF, et al. The surface molecular functionality of decellularized extracellular matrices. Biomaterials 2011;32:137–43.
[8] Brown BN, Barnes CA, Kasick RT, Michel R, Gilbert TW, Beer-Stolz D, et al. Surface characterization of extracellular matrix scaffolds. Biomaterials 2010;31:428–37.
[9] Hollander A, Macchiarini P, Gordijn B, Birchall M. The first stem cell-based tissue-engineered organ replacement: implications for regenerative medicine and society. Regener Med 2009;4:147–8.
[10] Macchiarini P, Jungebluth P, Go T, Asnaghi MA, Rees LE, Cogan TA, et al. Clinical transplantation of a tissue-engineered airway. Lancet 2008;372:2023–30.
[11] Elliott MJ, De Coppi P, Speggiorin S, Roebuck D, Butler CR, Samuel E, et al. Stem-cell-based, tissue engineered tracheal replacement in a child: a 2-year follow-up study. Lancet 2012;380:994–1000.
[12] Guo Y, Zeng Q, Yan Y, Shen L, Liu L, Li R, et al. Proliferative effect and osteoinductive potential of extracellular matrix coated on cell culture plates. SpringerPlus 2013;2:303.
[13] Decaris ML, Binder BY, Soicher M, Bhat A, Leach JK. Cell-derived matrix coatings for polymeric scaffolds. Tissue Eng Part A 2012;18:2148–57.
[14] Decaris ML, Leach JK. Design of experiments approach to engineer cell-secreted matrices for directing osteogenic differentiation. Ann Biomed Eng 2010;39:1174–85.
[15] Decaris ML, Mojadedi A, Bhat A, Leach JK. Transferable cell-secreted extracellular matrices enhance osteogenic differentiation. Acta Biomater 2012;8:744–52.
[16] Thibault RA, Scott Baggett L, Mikos AG, Kasper FK. Osteogenic differentiation of mesenchymal stem cells on pregenerated extracellular matrix scaffolds in the absence of osteogenic cell culture supplements. Tissue Eng Part A 2010;16:431–40.
[17] Tiwari A, Tursky ML, Kirkland MA, Pande G. Expansion of human hematopoietic stem/progenitor cells on decellularized matrix scaffolds. Curr Protoc Stem Cell Biol 2014;28. Unit1C.15.–1C.15.15..
[18] Prewitz MC, Seib FP, Bonin von M, Friedrichs J, Stißel A, Niehage C, et al. Tightly anchored tissue-mimetic matrices as instructive stem cell microenvironments. Nat Meth 2013;10:788–94.
[19] Chen LBL, Murray AA, Segal RAR, Bushnell AA, Walsh MLM. Studies on intercellular LETS glycoprotein matrices. Cell 1978;14:377–91.
[20] Soucy PA, Werbin J, Heinz W, Hoh JH, Romer LH. Microelastic properties of lung cell-derived extracellular matrix. Acta Biomater 2011;7:96–105.
[21] Rashid STS, Humphries JDJ, Byron AA, Dhar AA, Askari JAJ, Selley JNJ, et al. Proteomic analysis of extracellular matrix from the hepatic stellate cell line LX-2 identifies CYR61 and Wnt-5a as novel constituents of fibrotic liver. J Proteome Res 2012;11:4052–64.
[22] Bhat A, Boyadjiev SA, Senders CW, Leach JK. Differential growth factor adsorption to calvarial osteoblast-secreted extracellular matrices instructs osteoblastic behavior. PLoS ONE 2011;6:e25990.
[23] Reichert JC, Quent VMC, Burke LJ, Stansfield SH, Clements JA, Hutmacher DW. Mineralized human primary osteoblast matrices as a model system to analyse interactions of prostate cancer cells with the bone microenvironment. Biomaterials 2010;31:7928–36.
[24] Grünert M, Dombrowski C, Sadasivam M, Manton K, Cool SM, Nurcombe V. Isolation of a native osteoblast matrix with a specific affinity for BMP2. J Mol Histol 2007;38:393–404.
[25] Gospodarowicz DD, Delgado DD, Vlodavsky I. Permissive effect of the extracellular matrix on cell proliferation in vitro. PNAS 1980;77:4094–8.
[26] Evans ND, Gentleman E, Chen X, Roberts CJ, Polak JM, Stevens MM. Extracellular matrix-mediated osteogenic differentiation of murine embryonic stem cells. Biomaterials 2010;31:3244–52.
[27] Castelló-Cros R, Khan DR, Simons J, Valianou M, Cukierman E. Staged stromal extracellular 3D matrices differentially regulate breast cancer cell responses through PI3K and beta1-integrins. BMC Cancer 2009;9:94.
[28] Lee H-OH, Mullins SRS, Franco-Barraza JJ, Valianou MM, Cukierman EE, Cheng JDJ. FAP-overexpressing fibroblasts produce an extracellular matrix that enhances invasive velocity and directionality of pancreatic cancer cells. BMC Cancer 2011;11:245.
[29] Taubenberger AV, Quent VM, Thibaudeau L, Clements JA, Hutmacher DW. Delineating breast cancer cell interactions with engineered bone microenvironments. J Bone Miner Res 2013;28:1399–411.
[30] Clark AK, Taubenberger AV, Taylor RA, Niranjan B, Chea ZY, Zotenko E, et al. A bioengineered microenvironment to quantitatively measure the tumorigenic properties of cancer-associated fibroblasts in human prostate cancer. Biomaterials 2013;34:4777–85.
[31] Du P, Subbiah R, Park J-H, Park K. Vascular morphogenesis of human umbilical vein endothelial cells on cell-derived macromolecular matrix microenvironment. Tissue Eng Part A 2014;20:2365–77.
[32] Choi DH, Suhaeri M, Hwang MP, Kim IH, Han DK, Park K. Multi-lineage differentiation of human mesenchymal stromal cells on the biophysical microenvironment of cell-derived matrix. Cell Tissue Res 2014;357:781–92.
[33] Kutys ML, Doyle AD, Yamada KM. Regulation of cell adhesion and migration by cell-derived matrices. Exp Cell Res 2013;319:2434–9.
[34] Byron A, Humphries JD, Humphries MJ. Defining the extracellular matrix using proteomics. Int J Exp Pathol 2013;94:75–92.
[35] Soteriou D, Iskender B, Byron A, Humphries JD, Borg-Bartolo S, Haddock MC, et al. Comparative proteomic analysis of supportive and unsupportive extracellular matrix substrates for human embryonic stem cell maintenance. J Biol Chem 2013;288:18716–31.
[36] Welham NV, Chang Z, Smith LM, Frey BL. Proteomic analysis of a decellularized human vocal fold mucosa scaffold using 2D electrophoresis and high-resolution mass spectrometry. Biomaterials 2013;34:669–76.
[37] Wagner MS, Castner DG. Characterization of adsorbed protein films by time-of-flight secondary ion mass spectrometry with principal component analysis. Langmuir 2001;17:4649–60.
[38] Wagner MS, Horbett TA, Castner DG. Characterizing multicomponent adsorbed protein films using electron spectroscopy for chemical analysis, time-of-flight secondary ion mass spectrometry, and radiolabeling: capabilities and limitations. Biomaterials 2003;24:1897–908.
[39] Lhoest JB, Wagner MS, Tidwell CD, Castner DG. Characterization of adsorbed protein films by time of flight secondary ion mass spectrometry. J Biomed Mater Res 2001;57:432–40.

[40] Muramoto SS, Brison JJ, Castner DG. Exploring the surface sensitivity of TOF-secondary ion mass spectrometry by measuring the implantation and sampling depths of Bi_n and C_{60} ions in organic films. Anal Chem 2012;84:365–72.

[41] Baker MJ, Zheng L, Winograd N, Lockyer NP, Vickerman JC. Mass spectral imaging of glycophospholipids, cholesterol, and glycophorin a in model cell membranes. Langmuir 2008;24:11803–10.

[42] Lee C-Y, Harbers GM, Grainger DW, Gamble LJ, Castner DG, et al. Fluorescence, XPS and TOF-SIMS surface chemical state image analysis of DNA microarrays. J Am Chem Soc 2007;129:9429–38.

[43] Frisz JF, Choi JS, Wilson RL, Harley BAC, Kraft ML. Identifying differentiation stage of individual primary hematopoietic cells from mouse bone marrow by multivariate analysis of TOF-secondary ion mass spectrometry data. J Proteome Res 2012;84:4307–13.

[44] Barnes CA, Brison JJ, Robinson MM, Graham DJ, Castner DG, Ratner BD. Identifying individual cell types in heterogeneous cultures using secondary ion mass spectrometry imaging with C_{60} etching and multivariate analysis. Anal Chem 2012;84:893–900.

[45] Mains J, Wilson CG, Urquhart A. ToF-SIMS analysis of dexamethasone distribution in the isolated perfused eye. Invest Ophthalmol Vis Sci 2011;52:8413–9.

[46] Mains J, Wilson C, Urquhart A. ToF-SIMS analysis of ocular tissues reveals biochemical differentiation and drug distribution. Eur J Pharm Biopharm 2011;79:328–33.

[47] Sjövall P, Johansson B, Belazi D, Stenvinkel P, Lindholm B, Lausmaa J, et al. TOF-SIMS analysis of adipose tissue from patients with chronic kidney disease. Appl Surf Sci 2008;255:1177–80.

[48] Henss A, Rohnke M, Khassawna El T, Govindarajan P, Schlewitz G, Heiss C, et al. Applicability of ToF-SIMS for monitoring compositional changes in bone in a long-term animal model. J R Soc Interface 2013;10:20130332.

[49] Muramoto S, Rading D, Bush B, Gillen G, Castner DG. Low-temperature plasma for compositional depth profiling of crosslinking organic multilayers: comparison with C_{60} and giant argon gas cluster sources. Rapid Commun Mass Spectrom 2014;28:1971–8.

[50] Lee Chi-Ying, Gong Ping, Harbers Gregory M, Grainger David W, Castner David G, Gamble Lara J. Surface coverage and structure of mixed DNA/alkylthiol monolayers on gold: characterization by XPS, NEXAFS, and fluorescence intensity measurements. Anal Chem 2006;78:3316–25.

[51] Baugh L, Weidner T, Baio JE, Nguyen P-CT, Gamble LJ, Stayton PS, et al. Probing the orientation of surface-immobilized protein G B1 using ToF-SIMS, sum frequency generation, and NEXAFS spectroscopy. J Proteome Res 2010;26:16434–41.

[52] Mantus DS, Ratner BD, Carlson BA, Moulder JF. Static secondary ion mass spectrometry of adsorbed proteins. Anal Chem 1993;65:1431–8.

[53] Samuel NT, Wagner MS, Dornfeld KD, Castner DG. Analysis of poly(amino acids) by static time-of-flight secondary ion mass spectrometry (TOF-SIMS). Surf Sci Spectra 2001;8:163.

[54] Graham DJ, Castner DG. Multivariate analysis of ToF-SIMS data from multicomponent systems: the why, when, and how. Biointerphases 2012;7:49.

[55] Muramoto S, Graham DJ, Wagner MS, Lee TG, Moon DW, Castner DG. ToF-SIMS analysis of adsorbed proteins: principal component analysis of the primary ion species effect on the protein fragmentation patterns. J Phys Chem C Nanomater Interfaces 2011;115:24247–55.

[56] Canavan HE, Graham DJ, Cheng XX, Ratner BD, Castner DG. Comparison of native extracellular matrix with adsorbed protein films using secondary ion mass spectrometry. Langmuir 2007;23:50–6.

[57] Canavan HE, Cheng X, Graham DJ, Ratner BD, Castner DG. Surface characterization of the extracellular matrix remaining after cell detachment from a thermoresponsive polymer. Langmuir 2005;21:1949–55.

[58] Sidney LE, Kirkham GR, Buttery LD. Comparison of osteogenic differentiation of embryonic stem cells and primary osteoblasts revealed by responses to IL-1β, TNF-α, and IFN-γ. Stem Cells Dev 2014;23:605–17.

[59] Abdi H. The Bonferonni and Šidák corrections for multiple comparisons. In: Salkind N, editor. Encyclopedia of measurement and statistics. Thousand Oaks, CA: SAGE Publications; 2007. p. 1–9.

[60] Siow KS, Britcher L, Kumar SKS, Griesser HJ. Characterization of sulfate and phosphate containing plasma polymer surfaces. In: Nanoscience and nanotechnology, 2006 ICONN '06 international conference on 2006. p. 302–5.

[61] Lang FR, Pitton Y, Mathieu HJ, Landolt D, Moser EM. Surface analysis of polyethyleneterephthalate by ESCA and TOF-SIMS. Fresenius J Anal Chem 1997;358:251–4.

[62] Crapo PM, Gilbert TW, Badylak SF. An overview of tissue and whole organ decellularization processes. Biomaterials 2011;32:3233–43.

[63] Gospodarowicz D, Lui GM. Effect of substrata and fibroblast growth factor on the proliferation in vitro of bovine aortic endothelial cells. J Cell Physiol 1981;109:69–81.

[64] Hoshiba T, Kawazoe N, Tateishi T, Chen G. Development of stepwise osteogenesis-mimicking matrices for the regulation of mesenchymal stem cell functions. J Biol Chem 2009;284:31164–73.

[65] Hutmacher DW, Reichert JC, Clements JA, Burke LJ. Preparation of mineralised matrices secreted from human primary osteoblasts for analysis of the interaction of cancer cells and the bone microenvironment. Protoc Exch 2008.

[66] Mountziaris PM, Tzouanas SN, Mikos AG. The interplay of bone-like extracellular matrix and TNF-α signaling on in vitro osteogenic differentiation of mesenchymal stem cells. J Biomed Mater Res A 2012;2012(100):1097–106.

[67] Moursi AM, Damsky CH, Lull J, Zimmerman D, Doty SB, Aota S, et al. Fibronectin regulates calvarial osteoblast differentiation. J Cell Sci 1996;109:1369–80.

[68] Globus RK, Doty SB, Lull JC, Holmuhamedov E, Humphries MJ, Damsky CH. Fibronectin is a survival factor for differentiated osteoblasts. J Cell Sci 1998;111(Pt 10):1385–93.

[69] Canavan HE, Cheng X, Graham DJ, Ratner BD, Castner DG. Cell sheet detachment affects the extracellular matrix: a surface science study comparing thermal liftoff, enzymatic, and mechanical methods. J Biomed Mater Res A 2005;75A:1–13.

[70] Centrella MM, McCarthy TLT, Canalis EE. Tumor necrosis factor-alpha inhibits collagen synthesis and alkaline phosphatase activity independently of its effect on deoxyribonucleic acid synthesis in osteoblast-enriched bone cell cultures. Endocrinology 1988;123:1442–8.

[71] Rosenquist JB, Ohlin A, Lerner UH. Cytokine-induced inhibition of bone matrix proteins is not mediated by prostaglandins. Inflamm Res 1996;45:457–63.

[72] Ikeda E, Kusaka M, Hakeda Y, Yokota K, Kumegawa M, Yamamoto S. Effect of interleukin 1 beta on osteoblastic clone MC3T3-E1 cells. Calcif Tissue Int 1988;43:162–6.

[73] Smith DD, Gowen M, Mundy GR. Effects of interferon-gamma and other cytokines on collagen synthesis in fetal rat bone cultures. Endocrinology 1987;120:2494–9.

[74] Lu X, Gilbert L, He X, Rubin J, Nanes MS. Transcriptional regulation of the osterix (Osx, Sp7) promoter by tumor necrosis factor identifies disparate effects of mitogen-activated protein kinase and NF kappa B pathways. J Biol Chem 2006;281:6297–306.

[75] Gilbert LL, He XX, Farmer PP, Rubin JJ, Drissi HH, van Wijnen AJA, et al. Expression of the osteoblast differentiation factor RUNX2 (Cbfa1/AML3/Pebp2alpha A) is inhibited by tumor necrosis factor-alpha. J Biol Chem 2002;277:2695–701.

[76] Pischon NN, Darbois LML, Palamakumbura AHA, Kessler EE, Trackman PCP. Regulation of collagen deposition and lysyl oxidase by tumor necrosis factor-alpha in osteoblasts. J Biol Chem 2004;279:30060–5.

[77] Nanes MS. Tumor necrosis factor-α: molecular and cellular mechanisms in skeletal pathology. Gene 2003;321:1–15.

[78] Tsuboi M, Kawakami A, Nakashima T, Matsuoka N, Urayama S, Kawabe Y, et al. Tumor necrosis factor-alpha and interleukin-1beta increase the Fas-mediated apoptosis of human osteoblasts. J Lab Clin Med 1999;134:222–31.

[79] Tufvesson E, Westergren-Thorsson G. Alteration of proteoglycan synthesis in human lung fibroblasts induced by interleukin-1beta and tumor necrosis factor-alpha. J Cell Biochem 2000;77:298–309.

[80] Carvalho RS, Kostenuik PJ, Salih E, Bumann A, Gerstenfeld LC. Selective adhesion of osteoblastic cells to different integrin ligands induces osteopontin gene expression. Matrix Biol 2003;22:241–9.

[81] Humphries JD, Byron A, Humphries MJ. Integrin ligands at a glance. J Cell Sci 2006;119:3901–3.

[82] Dzamba BJ, Wu H, Jaenisch R, Peters DM. Fibronectin binding site in type I collagen regulates fibronectin fibril formation. J Cell Biol 1993;121:1165–72.

[83] Kubow KE, Conrad SK, Horwitz AR. Matrix microarchitecture and myosin II determine adhesion in 3D matrices. Curr Biol 2013;23:1607–19.

[84] Damianova R, Stefanova N, Cukierman E, Momchilova A, Pankov R. Three-dimensional matrix induces sustained activation of ERK1/2 via Src/Ras/Raf signaling pathway. Cell Biol Int 2008;32:229–34.

[85] Eyckmans J, Boudou T, Yu X, Chen CS. A hitchhiker's guide to mechanobiology. Dev Cell 2011;21:35–47.

[86] Reilly GC, Engler AJ. Intrinsic extracellular matrix properties regulate stem cell differentiation. J Biomech 2010;43:55–62.

[87] Kubow KE, Klotzsch E, Smith ML, Gourdon D, Little WC, Vogel V. Crosslinking of cell-derived 3D scaffolds up-regulates the stretching and unfolding of new extracellular matrix assembled by reseeded cells. Integr Biol (Camb) 2009;1:635–48.

[88] Pizzo AM, Kokini K, Vaughn LC, Waisner BZ, Voytik-Harbin SL. Extracellular matrix (ECM) microstructural composition regulates local cell–ECM biomechanics and fundamental fibroblast behavior: a multidimensional perspective. J Appl Physiol 2005;98:1909–21.

[89] Dumas V, Ducharne B, Perrier A, Fournier C, Guignandon A, Thomas M, et al. Extracellular matrix produced by osteoblasts cultured under low-magnitude, high-frequency stimulation is favourable to osteogenic differentiation of mesenchymal stem cells. Calcif Tissue Int 2010;87:351–64.

[90] Lehnert DD, Wehrle-Haller BB, David CC, Weiland UU, Ballestrem CC, Imhof BAB, et al. Cell behaviour on micropatterned substrata: limits of extracellular matrix geometry for spreading and adhesion. J Cell Sci 2004;117:41–52.

[91] Malmström JJ, Lovmand JJ, Kristensen SS, Sundh MM, Duch MM, Sutherland DSD. Focal complex maturation and bridging on 200 nm vitronectin but not fibronectin patches reveal different mechanisms of focal adhesion formation. Nano Lett 2011;11:2264–71.

[92] Wang J, Thampatty B. An introductory review of cell mechanobiology. Biomechan Model Mechanobiol 2006;5:1–16.

[93] Cukierman E, Pankov R, Stevens DR, Yamada KM. Taking cell–matrix adhesions to the third dimension. Science 2001;294:1708–12.

[94] Schwartz MA, Chen CS. Cell biology. Deconstructing dimensionality. Science 2013;339:402–4.